Maintaining flatness of a large aperture potassium bromide beamsplitter through mounting and vibration

Patricia Losch, James J. Lyons III

Optics Branch Code 551
NASA/Goddard Space Flight Center
Greenbelt, MD 20771

Armando Morell
NASA/Goddard Space Flight Center
Electromechanical Systems Branch Code 544
Greenbelt, MD 20771

Jim Heaney
Swales Aerospace
5050 Powder Mill Road
Beltsville, MD 20705

Abstract

The Composite Infrared Spectrometer (CIRS) instrument on the Cassini Mission launched in October of 1997. The CIRS instrument contains a mid-infrared (MIR) and a far-infrared interferometer (FIR) and operates at 170 Kelvin. The MIR is a Michelson Fourier transform spectrometer utilizing a 76 mm (3 inch) diameter potassium bromide beamsplitter and compensator pair. The potassium bromide elements were tested to verify effects of cooldown and vibration prior to integration into the instrument. The instrument was then aligned at ambient temperatures, tested cryogenically and re-verified after vibration. The stringent design optical figure requirements for the beamsplitter and compensator included fabrication errors, mounting stresses and vibration load effects. This paper describes the challenges encountered in mounting the elements to minimize distortion and to survive vibration.
Keywords: interferometry, Cassini, potassium bromide, infrared optics, cryogenic testing

1.0 Introduction

The CIRS is a remote sensor built at the Goddard Space Flight Center as an international collaboration with the European Space Agency[1]. CIRS was launched on NASA's Cassini Orbiter to Saturn in October 1997. Infrared spectroscopy of emissions from Saturn's and Titan's atmospheres, rings, and surfaces will provide 3-D and temporal variations of temperature distribution, gas abundances, aerosols, and clouds. Global mapping of Saturn's rings and icy satellite for composition and thermal properties will also be performed.[2]

CIRS consists of a 0.5 meter F/6 Cassegrain beryllium telescope, a reference interferometer to provide scan mechanism control and timing for data sampling, and two science Fourier transform spectrometers: a Mid-Infrared (MIR) interferometer and a Far infrared (FIR) interferometer. The MIR is a classical Michelson interferometer with a 7 - 17 micron spectral range measured with two linear HgCdTe arrays each consists of ten 200 micron square pixels each viewing 0.273 mrad field. The MIR detector arrays are centered about the telescope optical axis. The FIR is a polarizing Michelson interferometer measuring from 17 - 1000 microns using two 4.3 mrad thermopile detectors situated 4mrad off of the telescope optical axis.

CIRS is a passively cooled cryogenic instrument. All subsystems with the exception of the MIR focal plane operate at 170 Kelvin. The MIR focal plane operates at 80 Kelvin and is cooled using a honeycomb radiative patch.

The optical design of CIRS is described by Maymon et al[3]. A brief description of the optical layout of CIRS shown in Figure 1 is presented here. Light is collected across the 12.426 mrad field of view by the 0.5 meter, F/6

Cassegrain telescope. The beryllium telescope is mounted via a stress-free transition tube to the aluminum optics bench which houses the collimating optics and interferometers. A parabolic Entrance Aperture Plate (EAP) at the telescope focal surface serves to block stray light and is mounted in front of and to the field-split mirror. The EAP contains two apertures coincident with the MIR and FIR fields of view. The MIR and FIR fields of view are divided by the field split mirror which consists of two weak spherical mirrors each at 45° from the telescope optical axis. The FIR surface of the field split mirror was roughened and works in conjunction with a solar blocking filter to prevent solar radiation from traveling through the FIR interferometer and damaging the thermopile detectors. Both the MIR and FIR beams are then collimated by off-axis parabolas and steered into the interferometers via a fold flat in the MIR and an input polarizer for the FIR. The MIR contains a Potassium Bromide beamsplitter and compensator. The FIR utilizes a polarizing grid identical to the input polarizer (but rotated 45°) as its beamsplitter[4]. The fixed and moving mirrors are not typical flat mirrors but are cube corners in the MIR and dihedral mirrors in the FIR. These were developed at GSFC[5] to provide relief in the performance requirements of the mirror scanning mechanism. The dihedrals also serve to rotate the beams' polarizations. After passing through the fixed and moving legs of interferometer the MIR beam is focused onto the detector arrays by an F/1 germanium lens. The FIR beam is focused by an F/1 on-axis parabola through an output analyzer and onto the corresponding thermopile detectors[6]. Both signals are then Fourier transformed to provide spectral information.

Figure 1: CIRS Optical Layout

2.0 Beamsplitter Requirements

The choice of beamsplitter material was based on transmission characteristics between 600 and 1400cm^{-1}. In this region the two best candidates are potassium chloride and potassium bromide. Orignally KCl was the preferred choice because it is harder and less hydroscopic than KBr. However, KBr was chosen over KCl because of the transmission at 600cm^{-1}. At this wavelength KBr has a near unity transmission whereas KCl has a trnasmission of only about 0.5. The CIRS science team calculated that this reduced transmission would extend the required viewing time by a factor of 5 – 6, which was unacceptable. Observations at 600 cm^{-1} are associated with measuring the stratospheric CH_4 concentration for Saturn and Titan and for measuring the tropospheric temperatures of Saturn[7].

A flatness requirement for each beamsplitter and compensator surface was derived from the resulting effects on the modulation index of the MIR interferometer. The figure requirement was 0.125 waves peak-to-valley (p-v) and 0.025 waves root-mean-square (rms) where 1 wave = 633 nm. The transmission requirements for each compensator surface was ≥90% and for the non-beamsplitting surface of the beamsplitter it was ≥95%. The beamsplitting surface was to have the reflection and transmission equal to 50% ± 10%. The angles of incidence for the compensator and beamsplitter were approximately 37°. The minimum clear aperture of the optics defined an ellipse of major axis 65 mm and minor axis 48mm.

3.0 Engineering Unit

The engineering unit design attempted to minimize size and mass and therefore utilized the elliptical beam shape incident on the beamsplitter. The optical components were elliptically shaped with a major axis of 76 mm and a minor axis of 60 mm. The center thickness was 8.50 mm with a wedge of 0.06 degrees (to eliminate ghost images in the interferometer).

Problems arose from the start with this design. Although the optical elements were delivered with the correct major and minor axes dimensions, they were not true ellipses and did not fit into the mount housings which had been generated with computer numerically controlled machining methods. The components had to be returned to the vendor with the mount to have the edges ground down. The post edge grinding figures typically had a flatness of 0.33 waves peak to valley and 0.045 waves rms.

Another intrinsic problem with this design was the flatness of its housing's internal mounting surface. The optical components fit into a housing as shown in Figure 2. Each element is inserted from opposite sides of the housing and fits against a "lip" which maintains the separation of the components and provides a

wedge angle to eliminate ghost images in the interferometer. The elements are preloaded and retained into the housing via a wavy washer (i.e. spring) and a pressure plate as shown in Figure 3.

Figure 2: The optical housing for the beamsplitter and compensator

The inherent flaw of this design lies in the fact that there is no way to achieve an optically flat surface on the "lip" against which the KBr components are mounted. The KBr is an extremely soft material and is greatly influenced by the surface against which it is mounted. This same problem is amplified by the wavy washer torqued against it on the other side. This led to a final mounted figure error of 2.4 waves peak-to-valley and 0.42 rms.

Figure 3:Engineering Assembly drawing for the beamsplitter and compensator showing the wavy washer and pressure plate

Three different environmental tests were performed on the engineering unit components: cold "unmounted" figure error, cold mounted figure error and vibration.

The chamber used for all cryogenic figure error tests is shown in Figure 4. The 25cm diameter chamber uses a cryogenic transfer line to deliver liquid nitrogen (LN2) to the cold tip. The cold plate on which the optics are mounted bolts to this cold tip. A cylindrical thermal shroud also mounts to the cold tip and extends in length to the 20cm chamber window. The shroud accommodates various aperture plates which allows one to stop down the aperture to minimize heat load into the chamber. A Lakeshore Cryotronics Model 330 controller uses 50 ohm heaters (mounted on the cold plate) together with the adjustable LN2 flow rate to control the temperature. Platinum resistance thermometers are mounted on the cold plate and edge of the optic (or the housing in later tests) to monitor temperatures.

Figure 4: Cryogenic Test Chamber

The optics were first cold tested in an "unmounted" (unconstrained) configuration. The optic rested on two stainless steel pins and was retained with a small piece of thermally conductive tape. The flatness of the beamsplitter surface degraded by approximately 0.4 waves p-v and by 0.115 rms as compared to its ambient figure. The compensator degraded by 0.28 waves p-v and 0.06 waves rms.

The mounted cryogenic figure test (of the beamsplittiner surface) showed varying results. Initially at 170 Kelvin the figure had improved by 0.4 waves p-v and 0.15 rms compared to ambient. However for each subsequent warm measurement, the warm performance improved. While for each subsequent cold measurement, the cold performance was constant. A second series of cold cycles were performed at a later date. Once again the cold performance was constant and the warm data showed changes from cycle to cycle. At the end of the second series of cold cycles, the beamsplitter data at each temperature was repeating and showing a flatness degraded of 0.7 waves p-v and 0.17 waves rms. Although all the mount and housing components were heat treated as part of the fabrication process, we may have been observing some residual stresses being relieved.

The assembly was then vibrated in three axes on GSFC's Ling 335 vibration table. The assembly underwent both sinusoidal sweeps and random vibration at levels of 10g rms. These were qualification levels of vibration which were 25% greater than flight levels which in turn were greater than the limit loads calculated from conservative analysis. The assembly failed vibration when the beamsplitter cleaved into separate pieces along the crystal structure plane. The test was repeated and failed a second time in the same manner.

4.0 Flight Unit

4.1 Fight Unit Design

The flight housing design was modified from elliptical to circular in an attempt to rectify those problems effecting the engineering unit. The circular optics have a physical diameter of 77mm. The thickness of the optics remained at 8.50mm and had a clear aperture of 66mm.

Figure 5: Flight unit housing: note the raised pads on the internal surface.

The housing would no longer have a continuous surface or "lip" against which the elements were mounted but would have three diamond turned, optically flat pads. The wavy washer would be replaced with a retaining ring assembly. In this design, the ring has three pads underneath it which contact the optic opposite of the housing pads. The preload is set via clamps which depress the ring at points evenly spaced between the pads as shown in Figure 6.

Figure 6: Flight unit assembly: note the retaining ring, pads and clamps.

4.1 Fight Unit Performance

Three beamsplitter and compensator pairs were purchased for the flight unit. The delivered surface figure errors ranged from 0.45 to 0.93 waves p-v and 0.056 to 0.208 rms. The flatness of the housing's diamond turned pads was 2 waves p-v as measured over all three pads.

The figure degradation due to mounting ranged from 0 waves p-v and 0.007 rms to 0.2 waves p-v and 0.032 rms. The pre-vibration performance of the beamsplitter was 0.77 waves p-v and 0.124 rms and for the compensator, 0.615 waves p-v 0.063 rms.

The assembly was vibrated prior to cold testing because of past failures. The optics did not break during vibration and until we measured their figure, we assumed we had successfully passed the test. However, the beamsplitter showed a degradation of 0.4 waves p-v and 0.075rms – a change of 50%. The compensator's degradation was much worse with a post vibration error of 5.4 waves p-v and 1.203 rms – a change of 900% p-v and 100% rms!

A second beamsplitter/compensator pair was assembled using an increased spring constant for the retaining ring thus increasing the preload on the optical components. The pair was then vibrated. The degradation in beamsplitter figure was 1 wave p-v and 0.2 waves rms - a change of 120% p-v and 200% rms. For the compensator, the change was more than 3.7 waves p-v and .651 waves rms – a 300% change.

The sensitivity of the CIRS performance to these figure degradations was measured in the laboratory using the CIRS flight instrument. A mock-up focal plane assembly was used which consisted of an off-the-shelf F/2 germanium lens focusing onto single 1mm square HgCdTe detector. The vibrated beamsplitter and compensator pair were aligned into the MIR interferometer and interferometric scans were taken. An unvibrated assembly was then installed and aligned and the modulation index of the two beamsplitter/compensator pairs were compared. The major difference between these two pairs was the difference in compensator figures. No significant degradation was observed between the unvibrated set and the vibrated set. The reason that the large figure errors exhibited a low overall effect on the modulation index is due to stray light in the interferometer. This finding was confirmed by analysis of the CIRS instrument performance[8].

The vibrated set was then cold tested to check for temperature effects on the figures of the mounted optics. Data was taken at 160 Kelvin after soaking overnight. The beamsplitter showed an improvement of of 0.2 waves p-v and .068 waves rms and the compensator showed an improvement of 1.5 waves p-v and 0.2 waves rms. The warm and cold data repeated for this assembly.

We then subjected this same set to a second vibration to determine if the figure error would continue degrading due to the vibration. We found that the beamplitter again experienced a degradation of 46% p-v and 34%rms (0.9 waves p-v and 0.15 rms), whereas, the compensator degradation was only 0.3 waves p-v and 0.2 rms – change of 6% p-v and 15% rms.

Based on the interferometric performance data taken which showed minimal degradation of instrument performance with the vibrated optics, we utilized this design for flight.

5.0 Modified Design

In an attempt to understand the behavior of the KBr and our mount, we continued our testing after delivery of the CIRS instrument. A redesigned flight mount was developed which improved the stiffness of the cylindrical housing and accommodated optics with a lower diameter to thickness ratio. The improved stiffness was accomplished by adding flanges, supported by trusses, around each outer edge of the housing. The modified housing is shown in Figure 7. The retaining ring used was the same as that used for flight. The diameter of the optics remained the same (77mm) but the thickness of the optics was increased to from 8.5 to 11.2 mm.

Figure 7: Modified housing: note the additional flange around edge of housing for increased stiffness.

This assembly was then subjected to the same vibration environment as in previous tests. The figure degradation observed due to vibration was many times worse than that seen in the flight unit optics: a change of 900% for the beamsplitter and 400% for the compensator.

6.0 Experimental Design

At this point we wanted to separate the mount design from the optic (i.e. can a piece of KBr this size survive these vibration loads at all?). To this end, we built a relatively massive mount which is shown in Figure 8. The purpose of this design was to eliminate the mounting "ears" which attach the housing to the mounting bracket as used in previous designs. We felt that the ears may be transmitting deflections to the housing walls and warping the optical elements.

The experimental housing is shown in Figure 8. The assembly consisted of the mount with an internal lip, the compensator, a spacer ring, the beamsplitter, and a retaining ring. The retaining ring was secured via four 1/4 – 20 bolts. A thin, continuous ring of urelane was applied at every KBr to metal interface. Assembly took place while the compound was still soft resulting in a thin micro-layer of urelane. After the uralene had cured for 7 days, a preload of six pounds was applied, the bolts torqued and pre-vibration figure data was taken. The assembly was vibrated to the same levels as for each previous test. No degradation of the figure errors was observed.

Figure 8: Experimental housing : note the thick walls and the absence of mounting "ears".

6.0 Summary

We have been able to demonstrate that if properly mounted, a piece of KBr with an unsupported clear aperture of 66mm can survive severe vibration environments and maintain their figure at cold temperatures. For future work with large aperture KBr a design utilizing diamond turned mounting interfaces is feasible. Also, we have shown that the optimum housing to mounting bracket interface is not via three "ears". Our experiments suggest that a housing in which the ears are extended to define a continuous flange would eliminate warping of the optical elements.

7.0 Acknowledgments

The authors wish to thank Tom French, Lou Worell of NSI/ManTech, Carl Strojny, Ken Stewart, Marshall Space Flight Center, and Swales Aerospace.

8.0 References

1. Kunde, V. et al., "Cassini infrared Fourier spectroscopic investigation", Cassini/Huygens: A mission to the Saturnian Systems, Vol. 2803, SPIE, Denver, CO, 1996.

2. Kunde, V. et al., "Infrared spectroscopic remote sensing from the Cassini orbiter", Optical Spectroscopic Instrumentation and Techniques for the 1990s, Vol. 1318, SPIE, Las Cruces, NM, 1990.

3. Maymon et al., "Optical design of the Composite Infrared Spectrometer (CIRS) for the Cassini Mission", Space Astronomical Telescopes and Instruments II, Vol.1945, SPIE, Orlando, FL, 1993.

4. Crooke, J.A. et al., "Flight qualification of the Cassini-Composite Infrared Spectrometer (CIRS) - Far Infrared (FIR) polarizing beamsplitter substrate: Mylar chosen over Polypropylene", Cryogenic Optical Systems and Instruments VII, Vol.2814, SPIE, Denver, CO, 1996.

5. Lyons III, James Joseph , and Patricia Ann Hayes. "High Quality Cryogenic Hollow Retroreflectors", Current Developments in Optical Design and Engineering V, Vol. 2540, SPIE, San Diego, CA, 1995.

6. Crooke, J.A. and John G. Hagopian. "Alignment and Cryogenic Testing of the Cassini-Composite Infrared Spectrometer (CIRS) Far Infrared (FIR) Focal Plane", Cryogenic Optical Systems and Instruments VII, Vol.2814, SPIE, Denver, CO, 1996.

7. Virgil Kunde and Don Jennings "CIRS FIR Polarizer Substrate and MIR Beamsplitter and Compensator Substrate – Science Requirements", GSFC Internal Memo, June 18, 1993.

8. Martino, A.J. and John Hagopian. "Effects of shear defocus and wavefront error on the theoretical wavefront performance of CIRS", Cryogenic Optical Systems and Instruments VIII, Vol. 3435, SPIE, San Diego, CA, 1998.

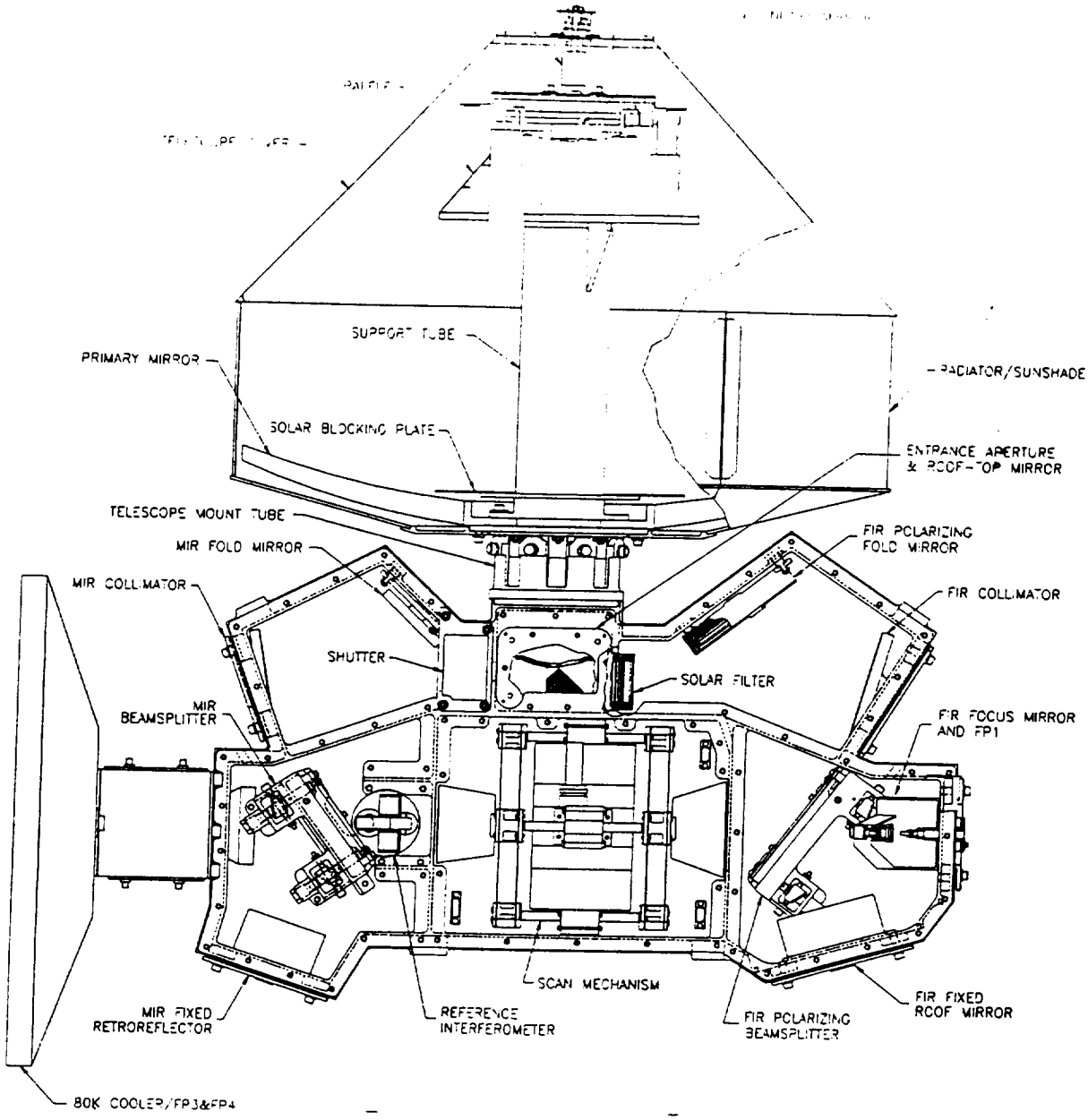
SUPPORT TUBE
PRIMARY MIRROR
RADIATOR/SUNSHADE
SOLAR BLOCKING PLATE
ENTRANCE APERTURE
& ROOF-TOP MIRROR
TELESCOPE MOUNT TUBE
MIR FOLD MIRROR
FIR POLARIZING
FOLD MIRROR
MIR COLLIMATOR
FIR COLLIMATOR
SHUTTER
SOLAR FILTER
MIR
BEAMSPLITTER
FIR FOCUS MIRROR
AND FP1
SCAN MECHANISM
MIR FIXED
RETROREFLECTOR
REFERENCE
INTERFEROMETER
FIR POLARIZING
BEAMSPLITTER
FIR FIXED
ROOF MIRROR
80K COOLER/FPJ&FP4

Fig 1

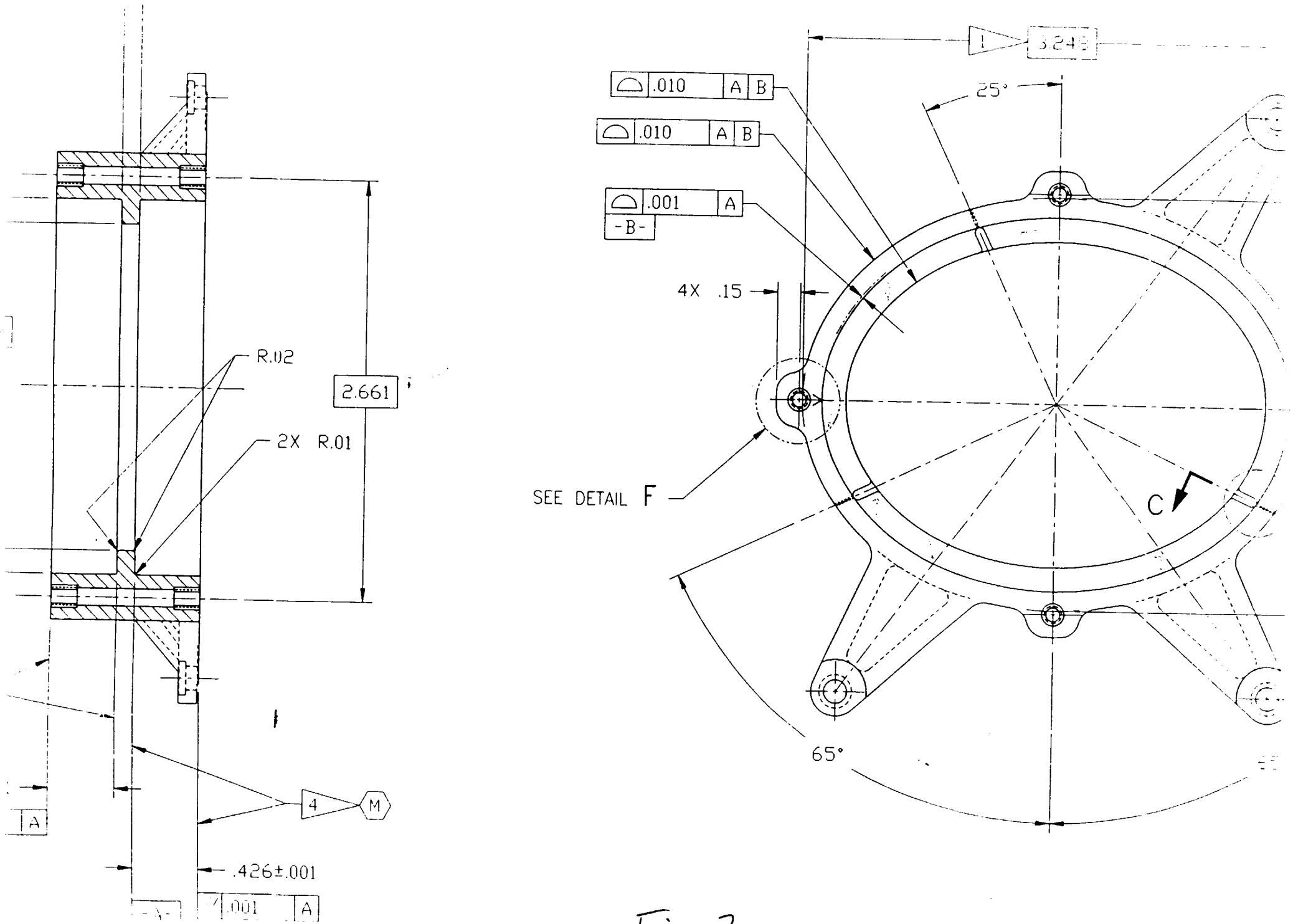
R.02
2.661
2X R.01
4
M
A
.426±.001
.001 A
.010 A B
.010 A B
.001 A
-B-
4X .15
SEE DETAIL F
25°
65°
C

Fig 2

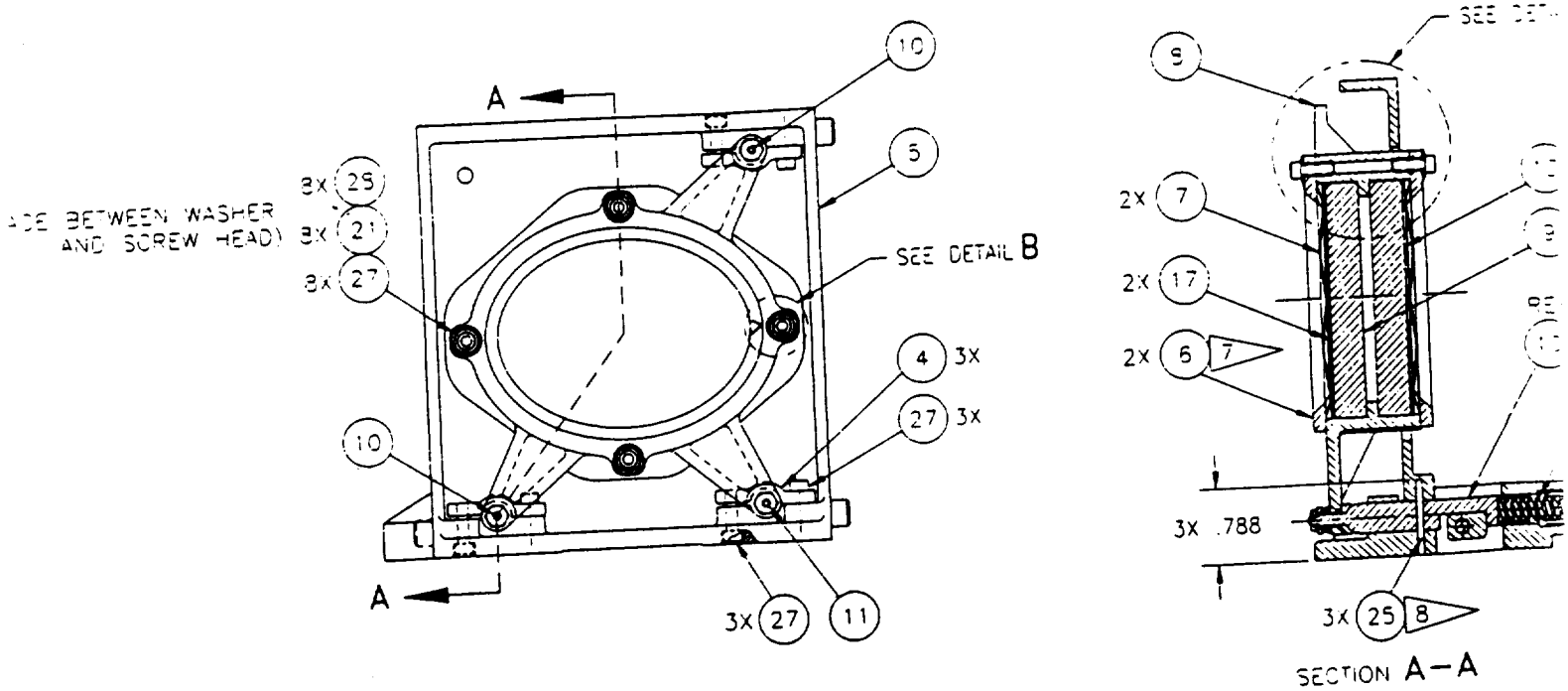
ADE BETWEEN WASHER AND SCREW HEAD)
8X 29
8X 21
8X 27
A
10
5
SEE DETAIL B
4 3X
27 3X
10
A
3X 27
11
SEE DET
9
2X 7
2X 17
2X 6
7
3X .788
3X 25
8
SECTION A–A

Fig 3

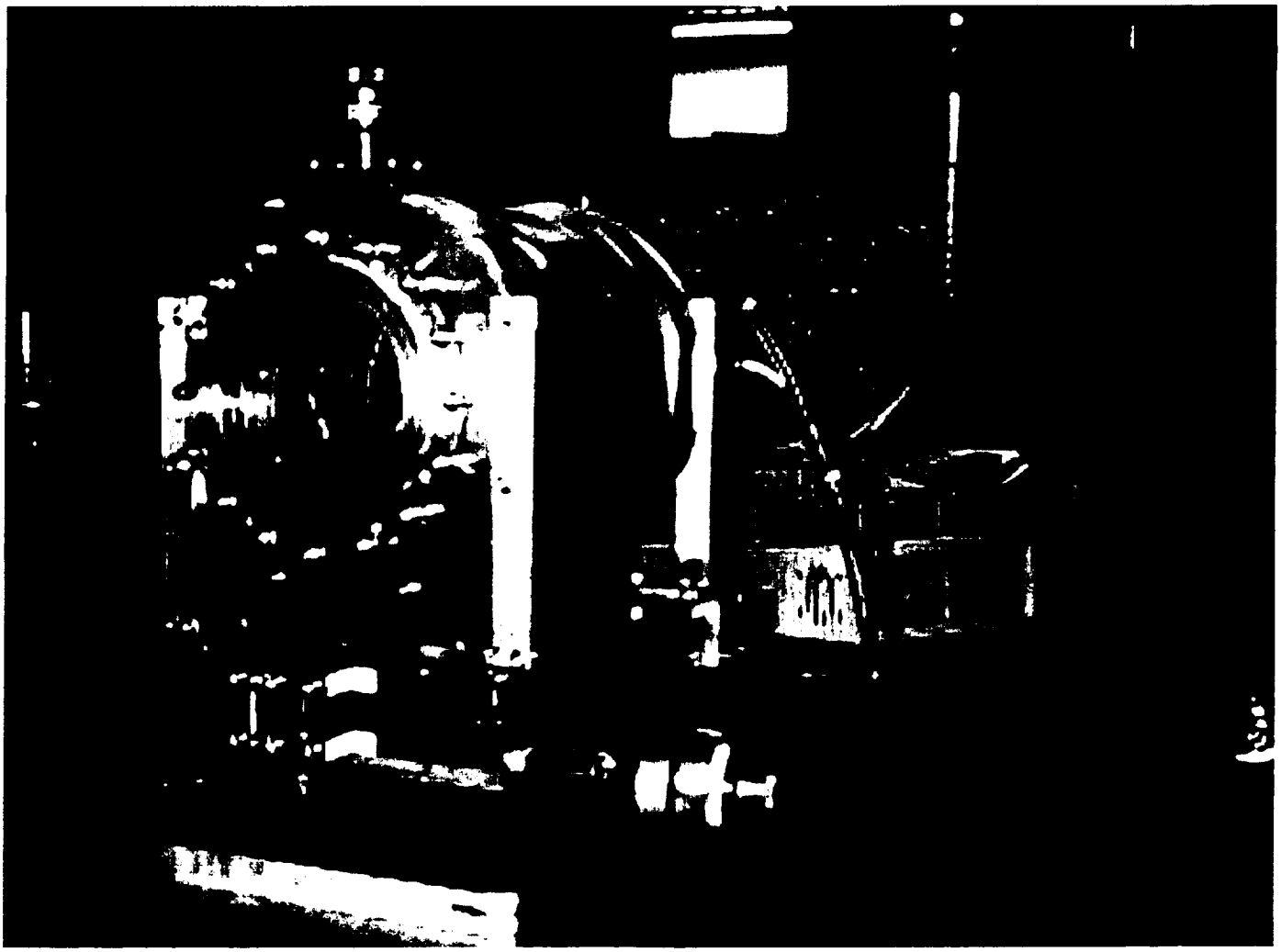

Fig 4

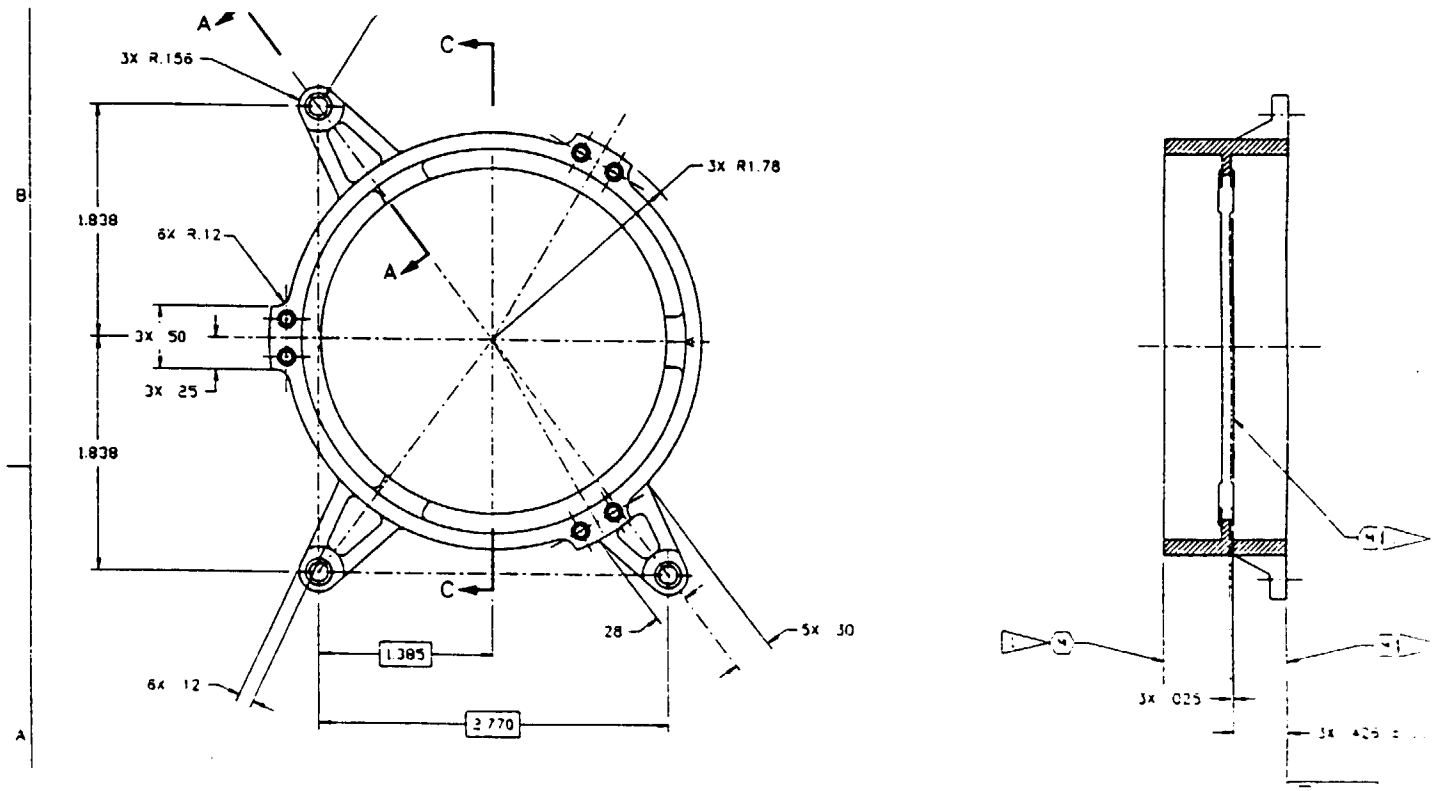
A
3X R.156
C
3X R1.78
B
1.838
6X R.12
A
3X 50
3X 25
1.838
C
28
5X 30
6X 12
1.385
2.770
3X Ø25

Fig 5

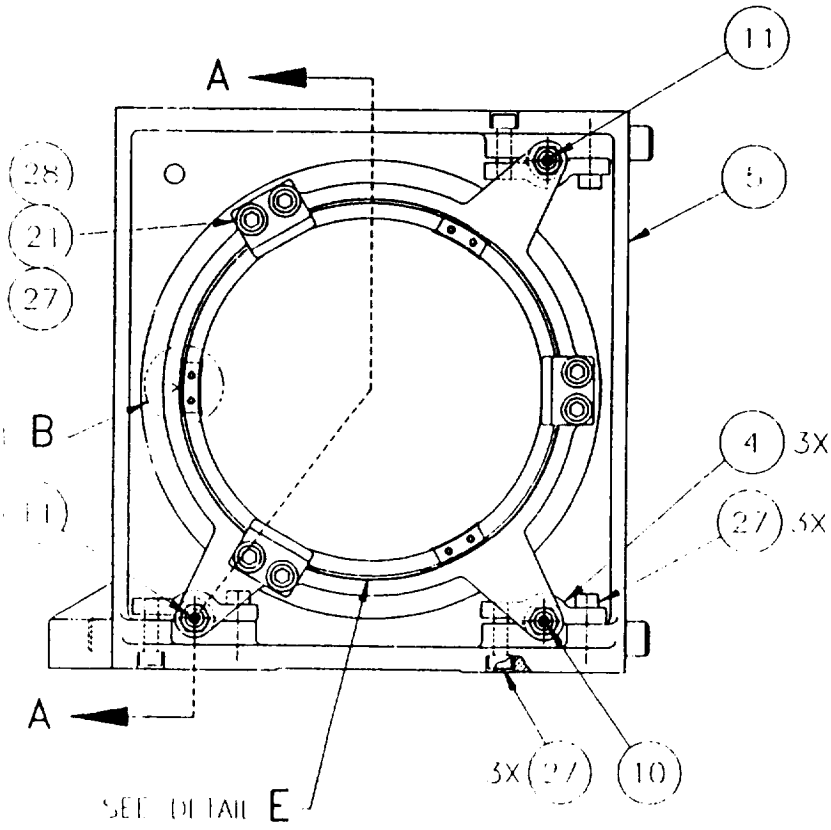
A
11
28
21
27
5
B
4 3X
27 3X
A
3X 27
10
SEE DETAIL E

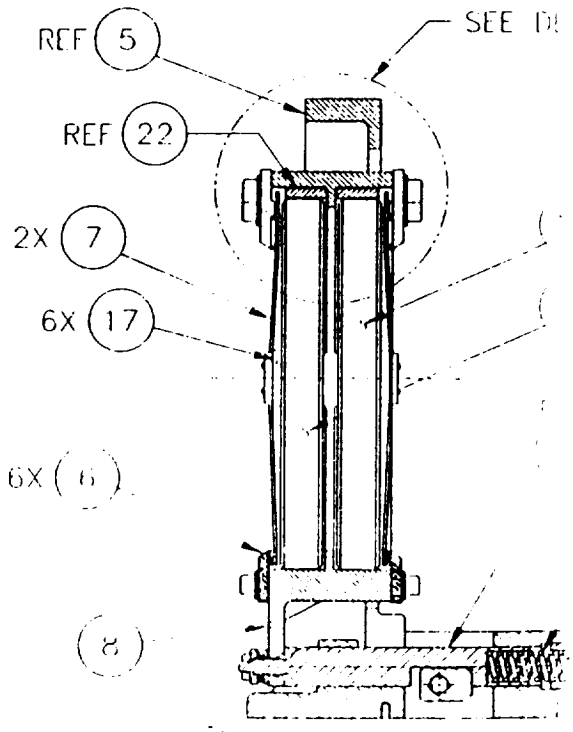
REF 5
SEE DE
REF 22
2X 7
6X 17
6X 6
8
SECTION A–A

Fig 6

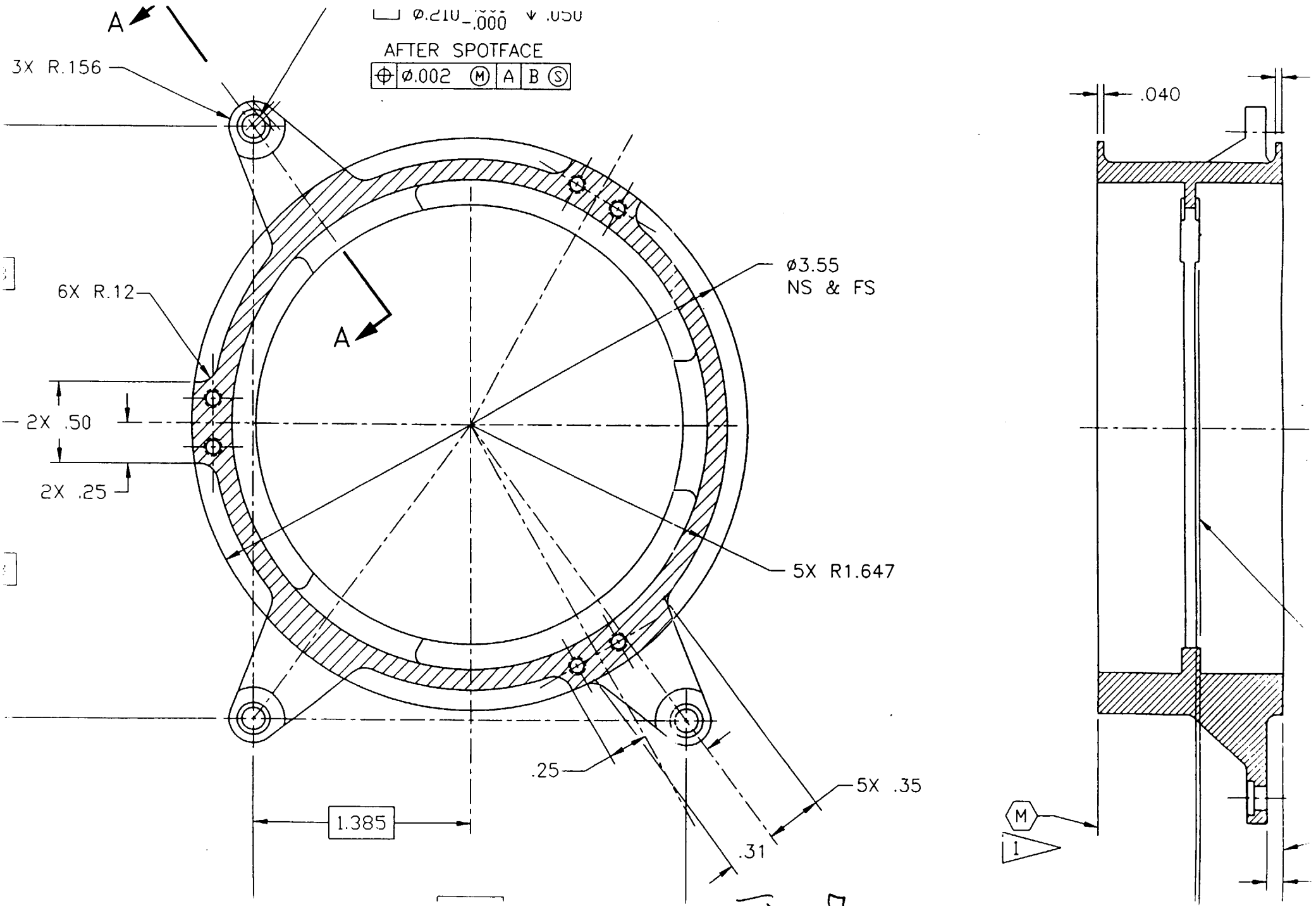
A
3X R.156
⌴ ø.210 -.000 ↧ .050
AFTER SPOTFACE
⌖ ø.002 Ⓜ A B Ⓢ
6X R.12
A
ø3.55
NS & FS
2X .50
2X .25
5X R1.647
.25
5X .35
1.385
.31
.040
M
1

Fig 7

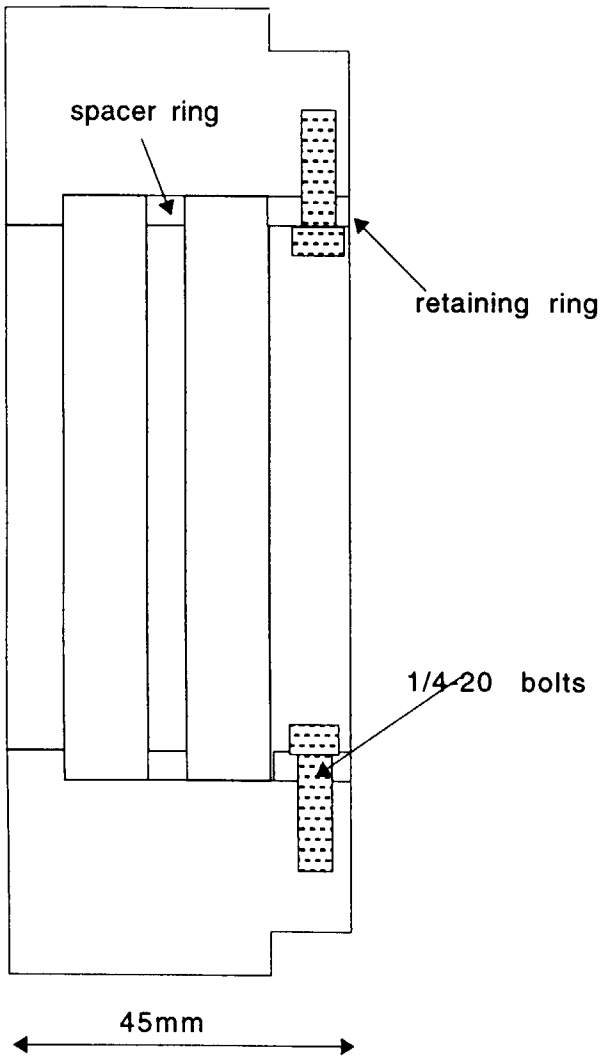
spacer ring
retaining ring
1/4-20 bolts
45mm

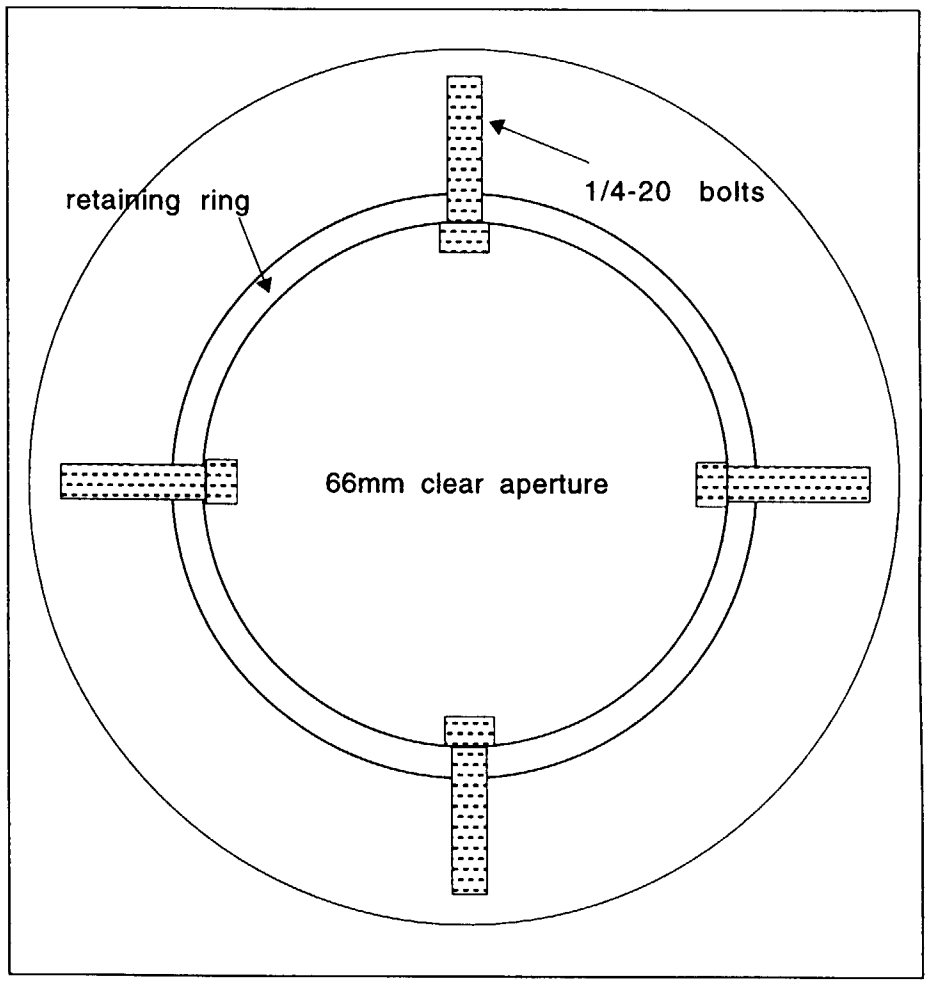
retaining ring
1/4-20 bolts
66mm clear aperture

Fig 8